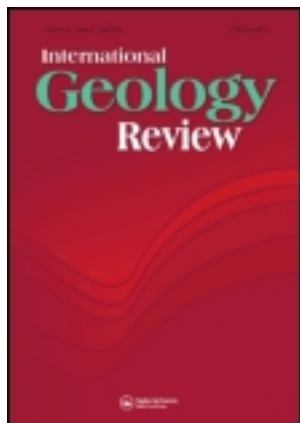


This article was downloaded by: [University of Ottawa]

On: 23 May 2012, At: 02:44

Publisher: Taylor & Francis

Informa Ltd Registered in England and Wales Registered Number: 1072954 Registered office: Mortimer House, 37-41 Mortimer Street, London W1T 3JH, UK



International Geology Review

Publication details, including instructions for authors and subscription information:

<http://www.tandfonline.com/loi/tigr20>

Origin of ultramafic xenoliths in high-Mg diorites from east-central China based on their oxidation state and abundance of platinum group elements

Jian Wang^a, Keiko Hattori^b, Wenliang Xu^a, Yongqiang Yang^c, Zhipeng Xie^a, Jinlin Liu^a & Yue Song^a

^a College of Earth Sciences, Jilin University, Changchun, Jilin, 130061, PR China

^b Department of Earth Sciences, University of Ottawa, Ottawa, ON, Canada, K1N 6N5

^c State Key Laboratory of Geological Processes and Mineral Resources, China University of Geosciences, Beijing, 100083, PR China

Available online: 08 Dec 2011

To cite this article: Jian Wang, Keiko Hattori, Wenliang Xu, Yongqiang Yang, Zhipeng Xie, Jinlin Liu & Yue Song (2012): Origin of ultramafic xenoliths in high-Mg diorites from east-central China based on their oxidation state and abundance of platinum group elements, *International Geology Review*, 54:10, 1203-1218

To link to this article: <http://dx.doi.org/10.1080/00206814.2011.628206>

PLEASE SCROLL DOWN FOR ARTICLE

Full terms and conditions of use: <http://www.tandfonline.com/page/terms-and-conditions>

This article may be used for research, teaching, and private study purposes. Any substantial or systematic reproduction, redistribution, reselling, loan, sub-licensing, systematic supply, or distribution in any form to anyone is expressly forbidden.

The publisher does not give any warranty express or implied or make any representation that the contents will be complete or accurate or up to date. The accuracy of any instructions, formulae, and drug doses should be independently verified with primary sources. The publisher shall not be liable for any loss, actions, claims, proceedings, demand, or costs or damages whatsoever or howsoever caused arising directly or indirectly in connection with or arising out of the use of this material.

Origin of ultramafic xenoliths in high-Mg diorites from east-central China based on their oxidation state and abundance of platinum group elements

Jian Wang^{a*}, Keiko Hattori^b, Wenliang Xu^a, Yongqiang Yang^c, Zhipeng Xie^a, Jinlin Liu^a and Yue Song^a

^aCollege of Earth Sciences, Jilin University, Changchun, Jilin 130061, PR China; ^bDepartment of Earth Sciences, University of Ottawa, Ottawa, ON, Canada, K1N 6N5; ^cState Key Laboratory of Geological Processes and Mineral Resources, China University of Geosciences, Beijing 100083, PR China

(Accepted 24 September 2011)

Ultramafic xenoliths are abundant in late Mesozoic high-Mg diorites at Laiwu, western Shandong Province; they are composed of dunite (>80 vol.%) with minor harzburgite (<10 vol.%) and olivine (Ol)-pyroxenite (<10 vol.%). We determined the abundance of siderophile and chalcophile elements of representative samples of xenoliths, and calculated oxidation conditions based on mineral chemistry. Bulk compositions of harzburgite show high Cr (2640–3430 ppm), Co (103–111 ppm), Ni (2210–2400 ppm), and high Ir-type platinum group elements (PGE) (IPGE, 14.0–17.8 ppb), with high ratios of IPGE to Pt-type PGE (PPGE, 3.1–6.3). Spinel contains moderate Cr ($Cr\# = 0.41\text{--}0.61$). Our data suggest that the harzburgite is the residue of partial melting. The occurrence of orthopyroxene replacing Ol suggests that harzburgite was metasomatized by a Si-rich melt. Dunite contains high concentrations of Cr (> 3800 ppm), Co (>110 ppm), and Ni (>1680 ppm), and low concentrations of IPGE (<4.8 ppb), with low ratios of IPGE/PPGE (as low as 0.05), suggesting that dunite is the cumulate of a mafic melt. High Cr in chromite ($Cr\# > 0.7$) and high Mg in Ol suggest that the parental melt was boninitic. Some Ol grains show variable, locally high Mg, up to Fo 94.3. We attribute these high values to the interaction of the Ol with abundant chromite in the cumulate. Both dunite and harzburgite indicate high $\log fO_2$ values, ranging from fayalite-magnetite-quartz (FMQ) +1.4 to +2.4. The values contrast with fO_2 below that of the graphite-CO₂ buffer for xenoliths in early Palaeozoic diamondiferous kimberlite pipes in the area. The data indicate a sharp increase in fO_2 during Mesozoic time, likely caused by subduction of the Tethyan oceanic plate before collision with the Yangtze continent below the eastern margin of the North China craton.

Keywords: late Mesozoic; subduction zone; PGE; fO_2 ; high-Mg diorite; dunite; ultramafic cumulate; subcontinental lithospheric mantle

Introduction

Late Mesozoic diorite intrusions occur in the Laiwu Basin on the eastern margin of the North China craton (NCC), along the Tan-Lu fault zone (Figure 1). The Laiwu area contains four high-Mg diorite plutons: the Kuangshan, Jiaoyu, Jinniushan, and Tietonggou intrusions. The Tietonggou body contains abundant ultramafic xenoliths, mainly dunite (>80%) with minor harzburgite and olivine (Ol)-pyroxenite. The origin of the dunite and its relationships to harzburgite and the host diorite have been debated. Proposed origins of the dunite include a residual mantle peridotite (e.g. Gao *et al.* 2008; Xu *et al.* 2008) and an accreted abyssal peridotite (Chen and Zhou 2005). The dunite may have other possible origins, including formation as a cumulate of a mafic melt (Leblanc and Ceuleneer 1992; Pagé and Barnes 2009; Shellnutt and Zellmer 2010), or a reaction product of harzburgite with a basaltic melt (Kelemen *et al.* 1990; Zhou *et al.* 1996, 1998).

We selected 11 representative ultramafic xenoliths at Tietonggou, including 2 harzburgite, 6 dunite, and 3 Ol-pyroxenite samples enclosed in the diorite intrusion, and determined mineral chemistry and the concentrations of chalcophile and siderophile elements in bulk rock samples. This article presents the results, evaluates the oxidation state indicated by mineral compositions, and discusses the origin of these xenoliths and the evolution of the subcontinental lithospheric mantle (SCLM) underlying the eastern margin of the NCC.

Geological setting

The NCC is an Archaean craton, bounded by the Northeast China Orogenic Belt, of late Palaeozoic age, to the north, the early Palaeozoic Qinling Orogenic Belt to the southwest, and by the Mesozoic Dabie-Sulu ultrahigh pressure (UHP) metamorphic belts to the south and east (e.g. Xiao

*Corresponding author. Email: wangjian304@jlu.edu.cn

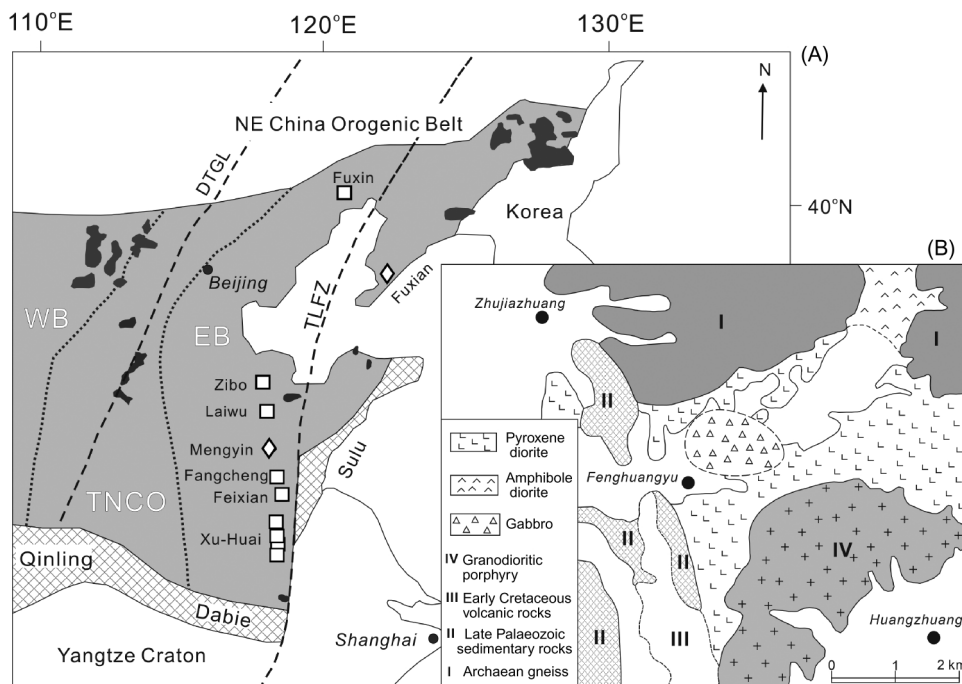


Figure 1. (A) Map of the North China Craton (NCC) showing the locations of the late Mesozoic high-Mg basalts and diorites of Fuxin, Zibo, Laiwu, Fangcheng, Feixian, and Xu-Huai (open squares), early Palaeozoic diamondiferous kimberlites of Mengyin and Fuxian (open diamonds), and Cenozoic basalts (dark areas). The NCC is divided by faults (thick dashed lines) into the Eastern Block (EB), Trans-North China Orogen (TNCO), and Western Block (WB). Thick dashed lines are the Daxinganling-Taihangshan Gravity Lineament (DTGL) and Tan-Lu Fault Zone (TLFZ), respectively. The map was modified after Zhao *et al.* (2001). (B) Geological map of the Laiwu area showing the Tietonggou high-Mg dioritic intrusion in western Shandong (modified after Xu *et al.* 2004a). Villages (solid circles) are shown with italics.

et al. 2003) (Figure 1). The Northeast China Orogenic Belt formed on the northern margin of the NCC during southward subduction of the Palaeo-Asian oceanic plate and the subsequent collision with the Siberia Craton, during the early Palaeozoic to Triassic (e.g. Xiao *et al.* 2003; Wu *et al.* 2011). The northward subduction of the Tethyan oceanic plate below the southern margin of the NCC was followed by collision of the Yangtze Craton; metamorphism of the subducted margin of the Yangtze Craton underwent peak metamorphism at ~ 220 Ma to form the Dabie-Sulu UHP belt (e.g. Li *et al.* 2007). After collision of the Yangtze and NCC cratons, the Palaeo-Pacific oceanic plate was subducted below the eastern margin of the Asian continent prior to ~ 150 Ma (e.g. Engebretson *et al.* 1985), producing numerous granitic intrusions in eastern China (Figure 1; Wu *et al.* 2011).

The NCC is divided into two portions, the Eastern and Western blocks, separated by the intervening Trans-North China Orogen, created at ~ 1.8 Ga (Figure 1; Zhao *et al.* 2001, 2005). The occurrence of harzburgite xenoliths in the Ordovician diamondiferous kimberlites at Mengyin and Fuxian (Figure 1; Zhang and Sun 2002, Zhang *et al.* 2008) in the Eastern Block suggests that the SCLM was thick (~ 200 km), cold, and refractory, similar to those beneath other Archaean cratons (Griffin *et al.* 1998). On the other hand, peridotite xenoliths from Cenozoic basalts indicate a

thin (< 80 km), hot, and fertile SCLM beneath the Eastern Block, implying that the SCLM in this area was thinned significantly (Fan *et al.* 2000; Kusky *et al.* 2007). The thinning process remains controversial, and the development of extensional basins in the area between the Tan-Lu fault zone and the Daxinganling-Taihangshan Gravity Lineament (Figure 1) suggest that this thinning occurred during the middle Mesozoic (Xu *et al.* 2004b; Zhai 2004; Wu *et al.* 2005; Kusky *et al.* 2007). Cretaceous high-Mg diorites and picritic basalts in the Eastern Block such as those in Feixian, Laiwu, Zibo, Fangcheng, and Fuxin (Figure 1), contain abundant ultramafic xenoliths (Zhang *et al.* 2002; Xu *et al.* 2003; Chen and Zhou 2005; Zheng *et al.* 2007; Gao *et al.* 2008). These xenoliths provide the information on the SCLM during the late Mesozoic.

The Laiwu basin, approximately $30 \text{ km} \times 50 \text{ km}$ in size, is underlain by Mesozoic and Cenozoic sedimentary rocks (Yang *et al.* 2004; Figure 1). High-Mg diorite plutons in the basin, less than 10 km^2 in size at the surface, contain moderate SiO_2 (54–60 wt.%) and show adakite-like geochemical features, such as high Sr/Y (up to 43) and La/Yb (up to 20) and low contents of heavy rare earth elements (REE) and Y (Yang 2008). High $^{87}\text{Sr}/^{86}\text{Sr}$ and low $^{143}\text{Nd}/^{144}\text{Nd}$ of the rocks suggest that they are formed by partial melting of the subducted Yangtze Craton and/or delaminated NCC (Xu *et al.* 2008; Yang 2008).

Samples

We studied representative samples of ultramafic xenoliths from the Tietonggou high-Mg dioritic intrusion in Laiwu (Figure 1). The xenoliths are round in shape and range in size from 1 to 8 cm in the longest dimension (Figure 2A). Dunite is predominant, accounting for >80 vol.% of xenoliths, with minor amounts of harzburgite (<10 vol.%) and Ol-pyroxenite (<10 vol.%).

Harzburgite commonly exhibits porphyroclastic and/or granoblastic textures of Ol (1–5 mm in size). Veins

of phlogopite- and/or amphibole-bearing orthopyroxenite occur in some xenoliths. Orthopyroxene grains (1–4 mm) are subhedral to anhedral and show the evidence of deformation. By contrast, orthopyroxene grains in veinlets (up to 1 cm in width) are small (0.1–0.5 mm) and show no evidence of deformation. Minor anhedral clinopyroxene crystals (1.0–1.5 mm) are also present in these veinlets. Cr-spinel is brown to reddish-brown under plain-polarized transmitted light; it is minor (<1 vol.%) and commonly shows vermicular intergrowth with Ol and orthopyroxene.

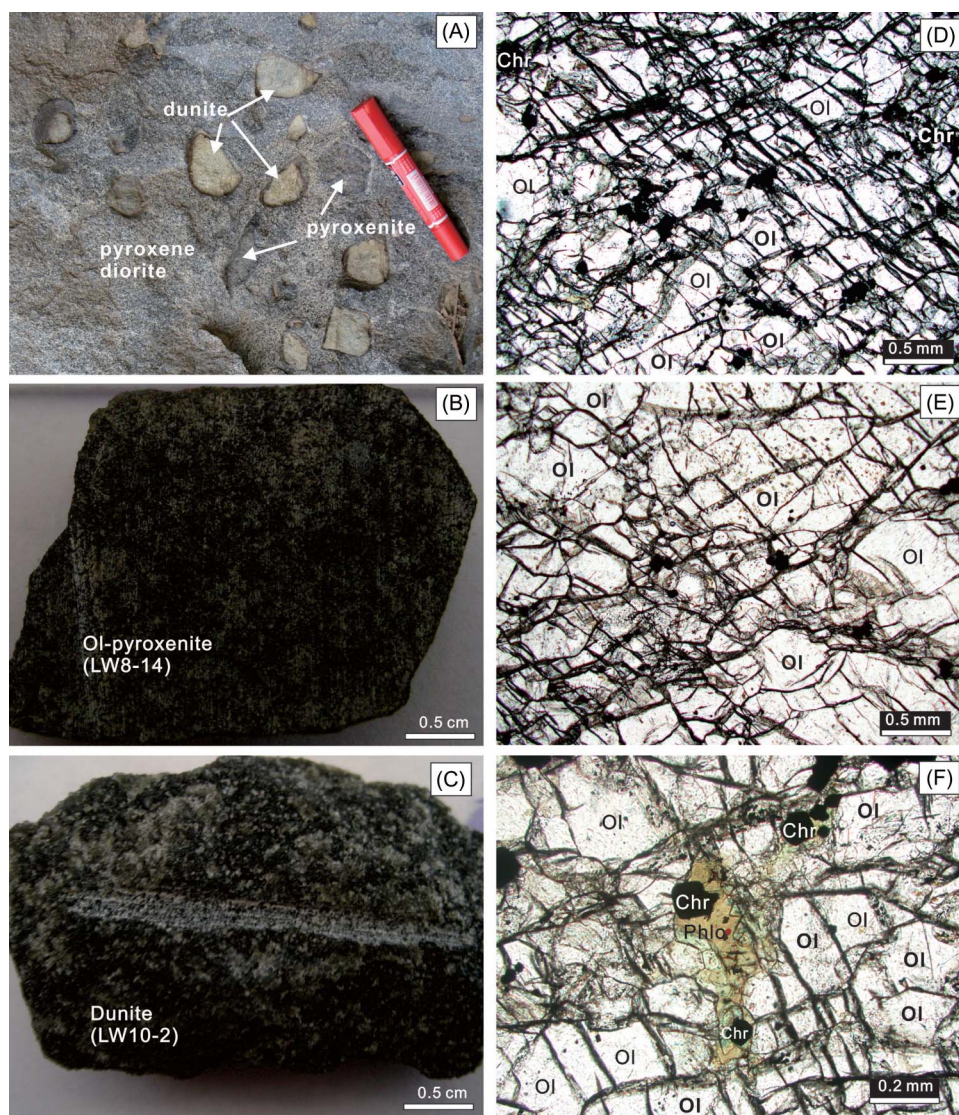


Figure 2. (A) Field photograph showing the occurrence of dunite and pyroxenite in the Laiwu pyroxene-diorite. (B) Photograph of a dark-coloured Ol-pyroxenite (sample LW8-14). (C) Photograph of typical dunite samples in the area (sample LW10-2). Note that the dunite is dark in appearance. (D) Photomicrograph of dunite under plain-polarized light (sample LW8-45). Grains of Ol are tabular and euhedral but chromite is either enclosed in Ol or at triple junctions of grain boundaries. Note the narrow veinlets of arrays of fluid inclusions, which contribute to the dark colour in hand specimens. (E) Photomicrograph of dunite under plain-polarized light (sample LW10-2). Grains of Ol show porphyroclastic texture. Tiny brown Cr-spinel inclusions are common in large Ol grains. Also common are net-like veinlets with diffusive boundaries cutting the sample. (F) Photomicrograph of dunite under plain-polarized light (sample LW8-45). Veinlet of phlogopite in the centre of the photomicrograph.

Dunite has an equigranular to cataclastic texture and consists of Ol (0.3–4 mm) and chromite (0.02–0.5 mm) (Figure 2D and Figure 2E). Ol has a bimodal size distribution: large porphyroclastic Ol (1–4 mm) and fine-grained Ol (0.3–0.6 mm). Aggregates of fine-grained Ol surround the large grains. Hand specimens of dunite are dark and foliated, as defined by tabular Ol crystals (Figure 2C). The dark colour is most likely due to abundant fluid inclusions within and along grain boundaries of Ol (Figure 2D and Figure 2E). Cr-spinel forms euhedral to subhedral grains and is typically enclosed in large Ol grains or occurs at the triple junction of Ol grains (Figure 2D and Figure 2E). Very small Cr-spinel grains also occur as inclusions in Ol crystals (Figure 2E). The modal abundance of chromite is highly variable, ranging from 10 to <1 vol.%. Orthopyroxene (0.02–0.2 mm), phlogopite (0.02–0.1 mm), and clinopyroxene (0.1 mm) are very minor, and occur as monomineralic veinlets (Figure 2F).

Pyroxenite includes both orthopyroxenite and websterite, with cumulate textures (Figure 2B). Minor Ol (<10 vol.%) is commonly present.

Analytical methods

Margins of xenoliths commonly show reaction rims on mineral boundaries, and were not used for analyses. Mineral compositions were determined using a JEOL JXA-8100 electron microprobe, in wavelength dispersive mode at the China University of Geosciences, Wuhan. Analytical conditions were 15 kV accelerating voltage, 20 nA beam current, and a focused beam diameter (<1 μm). Raw data were corrected using the ZAF method. The contents of Fe^{3+} in spinel were calculated assuming spinel stoichiometry. Compositions of individual minerals are similar within individual samples; representative compositions of minerals are listed in Table 1.

Contents of platinum group elements (PGE) were determined for 1–2 g samples by isotopic dilution using a mixed spike of ^{190}Os , ^{191}Ir , ^{99}Ru , ^{194}Pt , and ^{105}Pd after pre-concentration of PGE into a Ni-sulphide bead. The analytical procedures are similar to those described by Hattori and Guillot (2007). Mass ratios were determined using an Agilent HP-4500 ICP-MS at the University of Ottawa. Blank contributions were 0.002–0.006 ng Os/g flux, 0.002–0.007 ng Ir/g flux, 0.02 ng Ru/g flux, 0.07–0.16 ng Pt/g flux, and 0.03–0.12 ng Pd/g flux. The blanks are negligible compared to the amounts in samples; thus, blank corrections were not applied to the results. The analytical quality was monitored by running two rock references: TDB-1 diabase from CANMET, Natural Resources of Canada; and JP-1 harzburgite from the Geological Survey of Japan. The values for the two are comparable to those obtained by Meisel and Moser (2004) and Shirai *et al.* (2003) (Table 2).

The contents of Cu and S were determined using a Varian Vista-Pro inductively coupled plasma optical

emission spectrometer at the University of Ottawa after digestion of ~ 0.2 g of powder sample with aqua regia in a screw-top Teflon vial at $\sim 150^\circ\text{C}$ for 48 h. The precision based on replicate runs of five samples is <8% for Cu and <5% for S. The detection limits in solution are 0.004 ppm for Cu and 0.03 ppm for S, which is equivalent to 0.2 ppm for Cu and 1.4 ppm for S in solids.

Results

Bulk compositions

Two representative harzburgite samples were examined: sample T7-21 shows minor metasomatism, and sample LW8-44 is extensively metasomatized. Both contain high concentrations of MgO (>44 wt.%), Ni (>2200 ppm), Cr (>2600 ppm), and Co (>100 ppm). The compositions are similar to refractory mantle residues in many locations (e.g. Bell *et al.* 2005). Furthermore, they contain high Ir-type PGE (IPGE) and low Pt-type PGE (PPGE) and show a negatively sloped normalization pattern (Figure 3A). The pattern is similar to those of many mantle peridotites (Hattori and Guillot 2007; Saumur *et al.* 2011). Since IPGE remain in the mantle during partial melting whereas PPGE are preferentially incorporated in a melt (e.g. Richter *et al.* 2004; Brenan *et al.* 2005), the PGE pattern confirms that it is indeed a residual mantle peridotite after extensive partial melting.

The dunite contains high concentrations of compatible elements, such as MgO (>47 wt.%), Ni (>1700 ppm), Cr (>3800 ppm), and Co (>110 ppm), similar to values reported by Xu *et al.* (2008). The major element compositions are similar to those of residual mantle peridotites elsewhere, but the dunite samples contain low concentrations of IPGE (Os = 0.07–1.39 ppb, Ir = 0.24–0.50 ppb, Ru = 0.17–1.3 ppb) and high ratios of PPGE/IPGE (up to 22) (Table 2, Figure 4). The PGE pattern is similar to that of pyroxenites in the study area and Ural-Alaskan type ultramafic–mafic complexes along subduction zones (Figure 3B and Figure 3C; Garuti *et al.* 1997). Very low concentrations of IPGE in our dunite suggest that dunite is likely to be an ultramafic cumulate.

Mineral chemistry

Olivine

Ol in two harzburgite samples (T7-21, LW8-44) has moderately high Fo [$\text{Fo} = 100 \times \text{Mg}/(\text{Mg} + \text{Fe})$] ranging from 87.4 to 92.7 and NiO from 0.32 to 0.47 wt.%. The Fo value of 92.7 in sample T7-21 is similar to those of typical mantle peridotites, whereas extensively metasomatized sample LW8-44, with veinlets of orthopyroxenite and phlogopite, shows a low Fo value of 87.4 (Table 1A). The compositions obtained during this study are similar to those reported by previous workers (e.g. Chen and Zhou 2005; Xu *et al.* 2008).

Ol in dunite samples has high Fo (89.5–94.3) and NiO (0.20–0.45 wt.%; Table 1A), and the compositions of

Table 1. A. Representative composition of minerals (olivine and Cr-spinel) in ultramafic xenoliths from Laiwu, western Shandong.

Sample	T7-21	LW8-44	LW8-30	LW8-41	LW8-45	LW8-47	LW8-50	LW10-2	T7-15	T7-19
Lithology	Harzburgite		Dunite					Ol-pyroxenite		
olivine										
SiO ₂	41.27	39.83	40.56	40.82	40.83	41.65	41.27	41.11	40.85	40.99
TiO ₂	< 0.01	0.06	< 0.01	< 0.01	< 0.01	< 0.01	< 0.01	< 0.01	< 0.01	< 0.01
Al ₂ O ₃	< 0.01	< 0.01	0.03	0.05	0.03	0.01	0.02	0.02	< 0.01	< 0.01
Cr ₂ O ₃	< 0.02	0.01	0.04	0.04	< 0.02	< 0.02	0.02	< 0.02	< 0.02	< 0.02
FeO	7.22	12.20	9.75	7.69	9.34	5.64	8.70	8.82	12.94	15.70
MnO	0.12	0.11	0.18	0.12	0.20	0.04	0.08	0.15	0.29	0.36
MgO	50.99	47.56	49.25	51.14	50.11	52.89	50.36	49.41	45.78	42.89
NiO	0.47	0.32	0.30	0.33	0.20	0.45	0.29	0.27	0.00	0.00
CaO	0.02	0.01	0.02	0.04	0.04	0.01	0.04	0.04	< 0.02	0.03
Total	100.09	100.10	100.13	100.23	100.75	100.69	100.78	99.82	99.86	99.97
O = 4										
Si ⁴⁺	1.000	0.988	0.994	0.990	0.992	0.996	0.999	1.005	1.015	1.029
Ti ⁴⁺	0.000	0.001	0.000	0.000	0.000	0.000	0.000	0.000	0.000	0.000
Al ³⁺	0.000	0.000	0.001	0.001	0.001	0.000	0.001	0.001	0.000	0.000
Cr ³⁺	0.000	0.000	0.001	0.001	0.000	0.000	0.000	0.000	0.000	0.000
Fe ²⁺	0.146	0.253	0.200	0.156	0.190	0.113	0.176	0.180	0.269	0.330
Mn ²⁺	0.002	0.002	0.004	0.002	0.004	0.001	0.002	0.003	0.006	0.008
Mg ²⁺	1.842	1.759	1.799	1.850	1.815	1.885	1.817	1.800	1.695	1.605
Ni ²⁺	0.009	0.006	0.006	0.006	0.004	0.009	0.006	0.005	0.000	0.000
Ca ²⁺	0.001	0.000	0.001	0.001	0.001	0.000	0.001	0.001	0.000	0.001
Mg#	0.927	0.874	0.900	0.922	0.905	0.943	0.912	0.909	0.863	0.829
Sum	3.000	3.011	3.005	3.008	3.007	3.004	3.001	2.995	2.985	2.971
Cr-spinel/chromite										
SiO ₂	0.03	0.02	0.04	0.03	0.01	0.02	< 0.02	0.04		
TiO ₂	0.00	1.02	0.34	0.25	0.28	0.17	0.31	0.44		
Al ₂ O ₃	33.04	14.97	8.59	7.56	8.83	8.33	10.29	8.43		
Cr ₂ O ₃	33.66	34.24	51.61	54.30	47.12	59.45	50.01	50.88		
Fe ₂ O ₃	4.91	18.12	10.64	9.01	14.67	5.02	9.95	10.83		
FeO	13.69	20.24	20.86	19.37	20.72	13.83	22.73	20.30		
MnO	0.29	0.38	0.66	0.64	0.71	0.56	0.86	0.64		
MgO	15.34	8.94	8.07	8.70	7.88	12.33	6.89	8.20		
NiO	0.15	0.22	0.03	0.04	0.15	0.21	0.04	0.19		
Total	101.11	98.15	100.85	99.90	100.37	99.92	101.09	99.96		
O = 4										
Si ⁴⁺	0.001	0.001	0.001	0.001	0.000	0.001	0.000	0.001		
Ti ⁴⁺	0.000	0.026	0.009	0.006	0.007	0.004	0.008	0.011		
Al ³⁺	1.124	0.589	0.340	0.302	0.352	0.322	0.407	0.336		
Cr ³⁺	0.768	0.904	1.371	1.454	1.260	1.544	1.326	1.362		
Fe ³⁺	0.107	0.455	0.269	0.230	0.373	0.124	0.251	0.276		
Fe ²⁺	0.330	0.565	0.586	0.549	0.586	0.380	0.638	0.575		
Mn ²⁺	0.007	0.011	0.019	0.018	0.020	0.016	0.024	0.018		
Mg ²⁺	0.660	0.445	0.404	0.439	0.397	0.604	0.345	0.414		
Ni ²⁺	0.003	0.006	0.001	0.001	0.004	0.006	0.001	0.005		
Sum	3.000	3.002	3.000	3.000	2.999	3.001	3.000	2.998		
Cr#	0.41	0.61	0.80	0.83	0.78	0.83	0.77	0.80		
Mg#	0.67	0.44	0.41	0.44	0.40	0.61	0.35	0.42		

large porphyroclasts are similar to those of small grains in individual samples.

Spinel

Cr-spinel in harzburgite shows variable compositions even within one sample. Cr-spinel in the slightly metasomatized harzburgite (sample T7-21) shows moderate Cr# values

[= Cr/(Cr + Al)], ranging from 0.29 to 0.42 (Figure 5), whereas the highly metasomatized harzburgite sample LW8-44 has high values of Cr# (0.61–0.69) and $Fe^{3+}/(Al + Cr + Fe^{3+}) > 0.2$ (Figure 5A and Figure 5B).

In dunite, cores of coarse-grained spinel show similar composition within individual samples (Figure 5) and are characterized by relatively high Y_{Fe} (= $Fe^{3+}/(Al +$

Table 1. B. Representative composition of minerals (ortho- and clino-pyroxene) in ultramafic xenoliths from Laiwu, western Shandong.

Sample	T7-21		LW8-44		LW8-30		LW8-41		LW8-45		LW8-50		LW10-2		T7-15		T7-19		T7-21		LW8-44		LW8-41		LW8-45		LW8-47		T7-15			
	Harzburgite		Harzburgite		Harzburgite		Dunitite		Dunitite		Dunitite		Dunitite		Ol-pyroxenite		Ol-pyroxenite		Harzburgite		Harzburgite		Cpx		Cpx		Dunitite		Dunitite		Ol-pyroxenite	
Phase	Primary		Secondary ^b		Primary		Secondary ^b		Secondary ^b		Secondary ^b		Secondary ^b		Primary		Primary		Primary		Primary		Secondary ^b		Secondary ^b		Secondary ^b		Secondary ^b		Primary	
	Opx	Opx	Opx	Opx	Opx	Opx	Opx	Opx	Opx	Opx	Opx	Opx	Opx	Opx	Opx	Opx	Opx	Opx	Opx	Opx	Opx	Opx	Opx	Opx	Opx	Opx	Opx	Opx	Opx	Opx	Opx	
SiO ₂	56.32	56.51	57.33	57.89	57.33	57.89	56.21	56.21	58.08	56.69	56.69	57.45	56.56	54.62	54.29	56.13	54.73	53.24	56.14	56.14	56.14	53.24	53.24	53.24	53.24	53.24	53.24	53.24	53.24	53.24	56.14	
Al ₂ O ₃	2.88	1.43	0.73	0.22	0.73	0.22	0.68	0.68	< 0.02	0.58	0.58	0.88	1.55	1.35	1.49	0.29	1.21	2.50	1.81	1.81	1.81	2.50	2.50	2.50	2.50	2.50	2.50	2.50	2.50	2.50	1.81	
Fe ₂ O ₃ ^a	0.00	0.00	0.35	0.93	0.35	0.93	3.44	3.44	0.12	1.61	1.61	0.00	0.00	0.22	0.00	0.00	0.00	0.88	0.00	0.00	0.00	0.88	0.88	0.88	0.88	0.88	0.88	0.88	0.88	0.00		
TiO ₂	< 0.01	0.06	0.03	< 0.02	0.03	< 0.02	0.06	0.06	< 0.02	0.03	0.03	< 0.02	0.18	0.02	0.12	0.02	0.16	0.38	< 0.02	< 0.02	< 0.02	0.38	0.38	0.38	0.38	0.38	0.38	0.38	0.38	< 0.02		
Cr ₂ O ₃	0.57	0.44	0.17	0.07	0.17	0.07	0.34	0.34	0.24	0.35	0.35	0.38	0.13	0.24	0.60	0.20	1.01	1.34	0.27	0.27	0.27	1.34	1.34	1.34	1.34	1.34	1.34	1.34	0.27	0.27		
MgO	34.78	32.48	34.53	35.60	34.53	35.60	35.32	35.32	35.33	34.89	34.89	31.91	28.00	18.04	16.64	18.36	18.18	18.22	16.26	16.26	16.26	18.22	18.22	18.22	18.22	18.22	18.22	18.22	16.26	16.26		
FeO	4.97	7.51	6.14	4.81	6.14	4.81	3.06	3.06	5.62	4.75	4.75	8.13	12.05	1.62	2.71	2.11	2.82	1.02	4.91	4.91	4.91	1.02	1.02	1.02	1.02	1.02	1.02	1.02	4.91	4.91		
MnO	0.15	0.24	0.10	0.16	0.10	0.16	0.16	0.16	0.21	0.19	0.19	0.14	0.40	0.06	0.12	0.05	0.10	0.09	0.06	0.06	0.06	0.09	0.09	0.09	0.09	0.09	0.09	0.09	0.06	0.06		
CaO	0.25	0.45	0.50	0.53	0.50	0.53	0.58	0.58	0.34	0.37	0.37	0.51	1.22	23.75	23.25	23.47	21.66	22.02	19.95	19.95	19.95	22.02	22.02	22.02	22.02	22.02	22.02	22.02	19.95	19.95		
Na ₂ O	< 0.02	0.02	< 0.02	0.05	< 0.02	0.05	0.03	0.03	0.03	< 0.02	< 0.02	0.51	0.07	0.24	0.26	0.12	0.37	0.47	0.48	0.48	0.48	0.47	0.47	0.47	0.47	0.47	0.47	0.48	0.48	0.48		
Total	99.93	99.14	99.90	100.26	99.90	100.26	99.90	99.90	99.98	99.47	99.47	99.91	100.16	100.16	99.49	100.76	100.24	100.18	99.96	99.96	99.96	100.18	100.18	100.18	100.18	100.18	100.18	100.18	99.96	99.96		
O = 6																																
Si ⁴⁺	1.933	1.976	1.976	1.983	1.976	1.983	1.938	1.938	1.997	1.964	1.964	1.999	1.998	1.972	1.981	2.011	1.976	1.922	2.028	2.028	2.028	1.922	1.922	1.922	1.922	1.922	1.922	1.922	2.028	2.028		
Al ³⁺	0.117	0.059	0.030	0.009	0.030	0.009	0.028	0.028	0.000	0.024	0.024	0.036	0.065	0.057	0.064	0.012	0.052	0.106	0.077	0.077	0.077	0.106	0.106	0.106	0.106	0.106	0.106	0.106	0.077	0.077		
Fe ³⁺ ^a	0.000	0.000	0.009	0.024	0.009	0.024	0.089	0.089	0.003	0.042	0.042	0.000	0.000	0.006	0.000	0.000	0.000	0.024	0.000	0.000	0.000	0.024	0.024	0.024	0.024	0.024	0.024	0.024	0.000	0.000		
Ti ⁴⁺	0.000	0.002	0.001	0.000	0.001	0.000	0.002	0.002	0.000	0.001	0.001	0.000	0.005	0.001	0.003	0.001	0.004	0.010	0.000	0.000	0.000	0.010	0.010	0.010	0.010	0.010	0.010	0.010	0.000	0.000		
Cr ³⁺	0.015	0.012	0.005	0.002	0.005	0.002	0.009	0.009	0.007	0.010	0.010	0.010	0.004	0.007	0.017	0.006	0.029	0.038	0.008	0.008	0.008	0.038	0.038	0.038	0.038	0.038	0.038	0.038	0.008	0.008		
Mg ²⁺	1.779	1.693	1.777	1.818	1.777	1.818	1.815	1.815	1.811	1.801	1.801	1.655	1.475	0.971	0.905	0.980	0.979	0.980	0.876	0.876	0.876	0.980	0.980	0.980	0.980	0.980	0.980	0.876	0.876			
Fe ²⁺	0.143	0.220	0.177	0.138	0.177	0.138	0.088	0.088	0.161	0.137	0.137	0.237	0.356	0.049	0.083	0.063	0.085	0.031	0.148	0.148	0.148	0.031	0.031	0.031	0.031	0.031	0.031	0.148	0.148			
Mn ²⁺	0.004	0.007	0.003	0.005	0.003	0.005	0.005	0.005	0.006	0.006	0.006	0.004	0.012	0.002	0.004	0.002	0.003	0.003	0.002	0.002	0.002	0.003	0.003	0.003	0.003	0.003	0.003	0.002	0.002			
Ca ²⁺	0.009	0.017	0.018	0.019	0.018	0.019	0.021	0.021	0.013	0.014	0.014	0.019	0.046	0.919	0.909	0.901	0.838	0.852	0.772	0.772	0.772	0.852	0.852	0.852	0.852	0.852	0.852	0.772	0.772			
Na ⁺	0.000	0.001	0.000	0.003	0.000	0.003	0.002	0.002	0.002	0.000	0.000	0.034	0.005	0.017	0.018	0.008	0.026	0.033	0.034	0.034	0.034	0.033	0.033	0.033	0.033	0.033	0.033	0.034	0.034			
Sum	4.000	3.987	4.000	4.001	4.000	4.001	3.998	3.998	4.000	3.999	3.999	3.994	3.966	4.001	3.984	3.984	3.992	4.000	3.949	3.949	3.949	4.000	4.000	4.000	4.000	4.000	4.000	3.949	3.949			
Mg#	0.926	0.885	0.905	0.918	0.905	0.918	0.911	0.911	0.917	0.910	0.910	0.875	0.806	0.946	0.916	0.940	0.920	0.947	0.855	0.855	0.855	0.947	0.947	0.947	0.947	0.947	0.855	0.855				
Wo	0.47	0.88	0.91	0.96	0.91	0.96	1.09	1.09	0.65	0.72	0.72	0.99	2.45	47.4	47.92	46.35	44.06	45.73	42.98	42.98	42.98	45.73	45.73	45.73	45.73	45.73	42.98	42.98				
En	92.13	87.72	90.11	92.05	90.11	92.05	94.33	94.33	91.23	92.26	92.26	86.6	78.58	50.08	47.71	50.41	51.47	52.6	48.78	48.78	48.78	52.6	52.6	52.6	52.6	52.6	48.78	48.78				
Fs	7.41	11.4	8.98	6.99	8.98	6.99	4.57	4.57	8.11	7.02	7.02	12.4	18.97	2.53	4.38	3.24	4.47	1.66	8.24	8.24	8.24	1.66	1.66	1.66	1.66	1.66	8.24	8.24				

Note: ^aCalculated from the stoichiometric compositions; ^breplacing olivine.

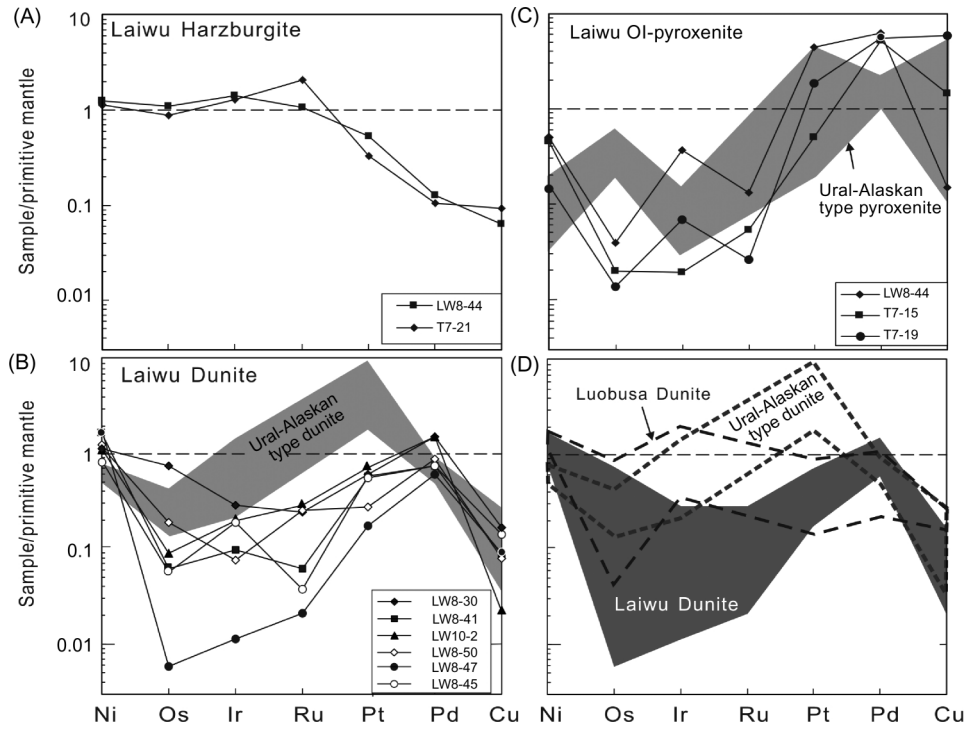


Figure 3. Primitive mantle-normalized PGE abundance in ultramafic xenoliths from Laiwu high-Mg diorites: (A) harzburgite, (B) dunite, (C) Ol-pyroxenite, and (D) comparison of the data for dunite from Laiwu (this study), Luobusa ultramafic–mafic complex in Tibet (Zhou *et al.* 1996), and Ural-Alaskan type mafic–ultramafic complexes along subduction zones (Garuti *et al.* 1997). Primitive mantle values are from McDonough and Sun (1995).

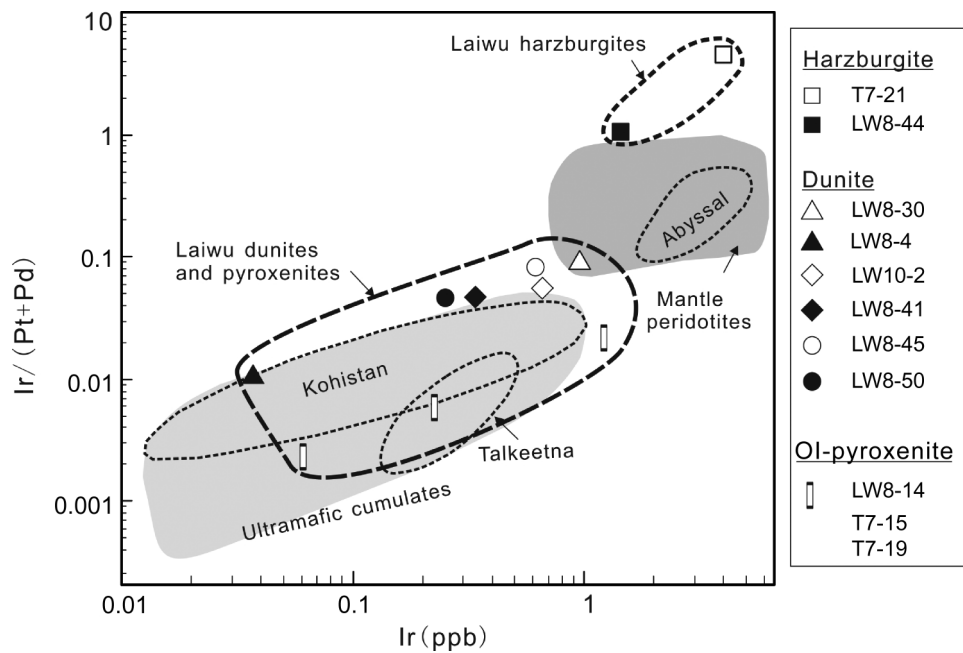


Figure 4. Ratios of Ir/(Pt + Pd) versus the contents of Ir (ppb) for Laiwu ultramafic xenoliths. The field for mantle peridotites includes abyssal peridotites (Rehkämper *et al.* 1999); Horoman, Japan (Rehkämper *et al.* 1999); Zabargad, Red Sea, and Ronda, Spain, plus forearc mantle serpentinites in Himalayas (Hattori and Guillot 2007). The field for ultramafic cumulates includes data from the Jijal ultramafic complex of the Kohistan Arc, Pakistan, and Talkeetna Arc (Hattori and Guillot 2007). Note that Laiwu harzburgite contains high Ir and plot in the field of mantle peridotites, whereas dunite is in the field partially overlapping with cumulates.

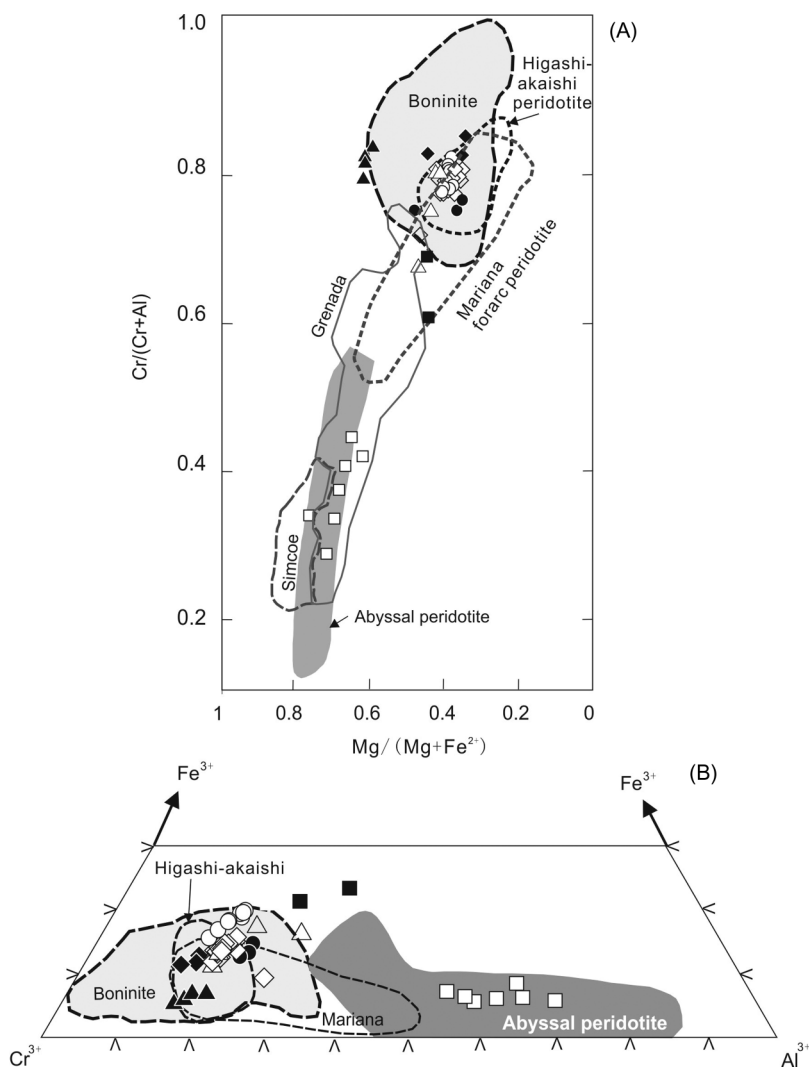


Figure 5. Binary $[\text{Cr}/(\text{Cr} + \text{Al})]$ vs. $\text{Mg}/(\text{Mg} + \text{Fe}^{2+})$ and ternary ($\text{Fe}^{3+}-\text{Cr}^{3+}-\text{Al}^{3+}$) diagrams for Cr-spinel in the Laiwu ultramafic xenoliths. Symbols are the same as in Figure 4. Each data point represents the core composition of one grain. Note that Cr-spinel grains in dunite have high Cr#, similar to those of Cr-spinel in boninites and forarc mantle peridotites. Cr-spinel in harzburgite shows variable Cr# even within one sample. Data sources: abyssal peridotites (Dick and Bullen 1984; Barnes and Roeder 2001), boninite (Barnes and Roeder 2001), Higashi-akaishi forearc peridotites (Hattori *et al.* 2010), Mariana forearc peridotites (Ishii *et al.* 1992), and Simcoe and Grenada subarc peridotites (Parkinson *et al.* 2003). Note that the compositions of spinel in boninite are similar to those of its source, forearc mantle peridotite.

Cr + Fe³⁺), 0.06–0.21, moderate Mg# [= $\text{Mg}/(\text{Mg} + \text{Fe}^{2+}) = 0.34\text{--}0.62$], and high Cr# >0.7 (Table 1A). The observed compositions are similar to those of chromites in boninite rocks (Barnes and Roeder 2001) and forearc mantle peridotites (e.g. Ishii *et al.* 1992; Hattori *et al.* 2010). The compositions are slightly higher in Cr# and lower in Mg# than those from subarc mantle peridotites (e.g. Brandon and Draper 1996; Parkinson and Arculus 1999; Parkinson *et al.* 2003) (Figure 4), and the Cr# is distinctly higher than those in abyssal peridotites (e.g. Dick and Bullen 1984) and in oceanic islands (Barnes and Roeder 2001); chromite in abyssal peridotites and oceanic islands

rarely shows values of Cr# >0.6 (Dick and Bullen 1984; Barnes and Roeder 2001).

Orthopyroxene

In harzburgite samples, orthopyroxene occurs as isolated primary grains and also as secondary grains replacing Ol. Mg# range from 0.89 to 0.93 and are characterized by relatively high contents of Al₂O₃ (1.43–2.88 wt.%) and Cr₂O₃ (0.40–0.57 wt.%) (Table 1B).

In dunite, orthopyroxene is secondary, forming bands around chromite and Ol, as well as veins with hydrous silicate minerals: the Al₂O₃ (0.22–1.21 wt.%) and Cr₂O₃

(0.07–0.5 wt.%) are relatively low, with a variable Mg# (0.91–0.97; Table 1B). A secondary origin of the orthopyroxene is supported by high concentrations of REE, up to 34 ppm in total (Xu *et al.* 2008). By contrast, the concentration of total REE rarely exceeds 1 ppm in mantle peridotites (e.g. Eggins *et al.* 1998).

Clinopyroxene

In harzburgite, clinopyroxene forms veins and also occurs as isolated grains. The isolated grains have high Mg# (0.91–0.95), which is in apparent equilibrium with Ol and orthopyroxene in individual samples (Table 1B). Clinopyroxene is rare in dunite and only found in several samples (LW8-41, LW8-45, and LW8-47), where it forms veins. Its compositions are variable between different grains.

Ol-bearing pyroxenite (T7-15, T7-19, LW8-14) contains low-Mg Ol (Fo = 80–86), orthopyroxene (Mg# = 0.81–0.87), and clinopyroxene (Mg# = ~0.86) (Table 1B); these data are consistent with a cumulate origin.

Oxidation state of samples

We have evaluated the oxidation state of the SCLM underlying the study area using the spinel–Ol–orthopyroxene oxybarometry and the Ol–spinel Fe–Mg exchange thermometry of Ballhaus *et al.* (1991). The calculated values are expressed relative to the fayalite–magnetite–quartz (FMQ) buffer (in logarithmic terms). In dunite, a minor variation in the Fe³⁺ content in spinel grains yielded slightly different fO_2 values, but the range is less than 0.3 logarithmic units in individual samples (Table 3). Grains of spinel and Ol in apparent textural equilibrium were selected for calculation of fO_2 ; and the values vary by less than 0.4 logarithmic units in individual samples (Table 3).

Both dunite and highly metasomatized harzburgite samples yielded high fO_2 values, ranging from FMQ +1.4 to +2.4 (median at FMQ +2.0). High- fO_2 values may possibly be attributed to equilibration with the host diorite during the entrainment by the intrusion, but we discount this possibility because the mineral chemistry of the xenoliths is not equilibrated with those in the host diorite. For example, the equilibrium temperatures calculated from mineral chemistry show high temperatures for diorite compared to those for harzburgite and dunite. The two-pyroxene thermometry of Wells (1977) gives 890–915°C for harzburgite and 910–940°C for dunite, and Ca-in-Opx thermometry of Brey and Köhler (1990) indicates 790–940°C for harzburgite and 860–950°C for dunite. These values are significantly lower than the temperatures for the host diorite of 1083°C, based on the two-pyroxene thermometry, and 1164°C using the Ca-in-Opx thermometry (Xu *et al.* 2008). This evidence suggests little interaction between xenoliths and host diorite, and thus implies that the oxidized state calculated from mineral chemistry in the

xenoliths most likely reflects the conditions of peridotites before the entrapment in the dioritic magma.

Harzburgite shows a variation in fO_2 ; a highly metasomatized sample shows high fO_2 similar to that for dunite (Table 3). The data suggest that the melt responsible for metasomatism had a high fO_2 , and that the SCLM was oxidized during metasomatism.

Discussion

Oxidation state of the late Mesozoic mantle

The fO_2 values obtained for our dunite and metasomatized harzburgite samples are similar to those of arc cumulates (e.g. Ballhaus 1993) and subarc mantle peridotites (Brandon and Draper 1996; Parkinson and Arculus 1999; Parkinson *et al.* 2003; Figure 6, Table 3). The values are distinctly higher than those of SCLM underlying ancient cratons, such as Kaapvaal craton (e.g. Woodland and Koch 2003; McCammon and Kopylova 2004).

The presence of diamondiferous kimberlites in the area (Figure 1) suggests that the SCLM was reduced, with an fO_2 value below the graphite–CO₂ buffer in early Palaeozoic time. This implies that the mantle was oxidized sometime between early Palaeozoic and late Mesozoic times. The tectonic activity that may have affected the oxidation state of the SCLM includes (1) upwelling of the asthenospheric mantle in Mesozoic time, (2) subduction of the Tethyan oceanic plate, (3) subduction of the northern margin of the Yangtze Craton during the Mesozoic, and (4) westward subduction of the Palaeo-Pacific plate in late Mesozoic time. Among these possibilities, the upwelling of the asthenospheric mantle is unlikely to have raised fO_2 because it has an fO_2 near the FMQ buffer (Bryndzia and Wood 1990; Ballhaus 1993; Wang *et al.* 2008a). The subduction of the Palaeo-Pacific oceanic plate (possibility 4) is unlikely to have contributed to a high fO_2 in the study area because the area is west of the Sulu UHP belt, which is the collision zone of the Yangtze Craton and NCC (Figure 1). The Sulu belt is likely to have acted as a physical barrier for the subducted Palaeo-Pacific oceanic plate as the collision zone has a depth of at least 200 km (Ye *et al.* 2000; Zhang and Liou 2003; Liu *et al.* 2007). Therefore, we propose that subduction of the Tethyan oceanic plate is likely to have raised fO_2 to the observed level. It is also possible that the subduction of the margin of the Yangtze Craton may have contributed to this oxidation because continental margins are commonly covered by oxidized shallow-water sediments, such as evaporates.

Origin of peridotite xenoliths

Origin of harzburgite

High Cr (2640–3430 ppm), Co (103–111 ppm), Ni (2210–2400 ppm), and IPGE (Os + Ir + Ru = 14.0–17.8 ppb), and high ratios of IPGE/PPGE in bulk rocks,

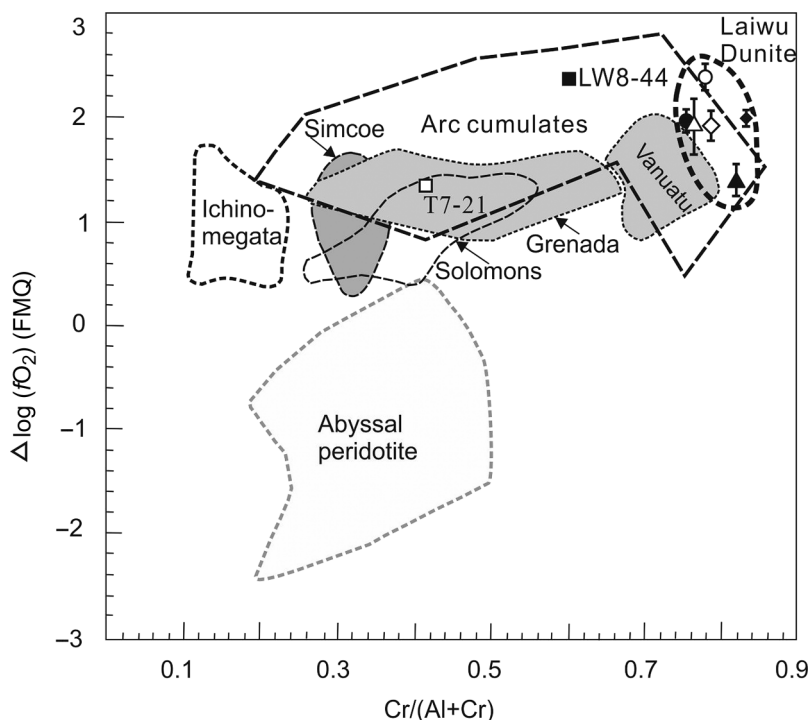


Figure 6. Values of fO_2 relative to the FMQ buffer, $\log fO_2$ (FMQ) versus Cr# in spinel for Laiwu ultramafic xenoliths compared with arc cumulates (Ballhaus 1993), abyssal peridotites (Bryndzia and Wood 1990), and xenoliths of subarc mantle peridotites at Simcoe (Brandon and Draper 1996); Ichinomegata, Japan (Wood and Virgo 1989; Parkinson and Arculus 1999); Grenada, Marelava, and Solomons (Parkinson and Arculus 1999; Parkinson *et al.* 2003). Symbols are the same as in Figure 4.

Table 3. Estimated oxygen fugacity values for the ultramafic Xenoliths from Laiwu high-Mg diorites, western Shandong.

sample	T7-21	LW8-44	LW8-30	Lw8-41	LW8-45	LW8-47	LW8-50	LW10-2
Lithology	Harzburgite			Dunite				
<i>Olivine</i>								
X_{Fe}^{Ol}	0.073	0.126	0.100	0.078	0.095	0.057	0.088	0.091
X_{Mg}^{Ol}	0.927	0.874	0.900	0.922	0.905	0.943	0.912	0.909
<i>Spinel</i>								
Cr#	0.289–0.444	0.605–0.688	0.759	0.835	0.781	0.821	0.756	0.789
$Fe^{3+}/\Sigma Fe$	0.245–0.418	0.429–0.446	0.344	0.279	0.373	0.252	0.313	0.306
$K_D^{(Mg-Fe)Ol-Sp^a}$	3.888–7.839	8.827–8.734	11.76	19.70	14.88	10.70	16.07	15.67
$T(^{\circ}C)^b$	710 ± 50	820 ± 20	760	670	730	810	690	700
$\Delta \log(fO_2)^{FMQ^c}$	1.33 ± 0.12	2.24 ± 0.12	1.88 ± 0.28	1.99 ± 0.08	2.39 ± 0.14	1.39 ± 0.18	2.00 ± 0.11	1.93 ± 0.13

Notes: ^aFe-Mg distribution coefficient between olivine and spinel.

^bCalculated based on Ol-Spl exchange thermometer of Ballhaus *et al.* (1991).

^c fO_2 estimates following the method of Ballhaus *et al.* (1991) using Fe^{3+} contents of spinel calculated from its stoichiometric composition and assuming the pressures at 1.5GPa.

suggest that the harzburgites in the area are compositionally refractory and similar to those typical mantle residues (e.g. Rehkämper *et al.* 1999). The refractory nature of harzburgite is also supported by high Mg contents of primary silicate minerals and the high Cr# of spinel (Table 1). Therefore, both bulk compositions and mineral chemistry suggest that harzburgite represents mantle residue after partial melting. The melting may have taken place during

the Archaean, considering the Re-depletion model ages of these harzburgite samples (LW8-44: 2.7 Ga; and T7-21: 2.6 Ga; Gao *et al.* 2008).

Harzburgite underwent cryptic and modal metasomatism and gained Si and lost Mg. The metasomatic agent was most likely a melt because of the occurrence of high-Ti phlogopite and amphibole; Ti is considered to be not mobile in fluids.

Origin of dunite

Possible origins of dunite include (1) residue after extensive partial melting (Kubo 2002), (2) a reaction product between peridotite and hydrous mafic melt (Zhou *et al.* 1996, 1998), and (3) a cumulate of a mafic melt (e.g. Leblanc and Ceuleneer 1992). First, a refractory mantle origin (Gao *et al.* 2008; Xu *et al.* 2008) is supported by the high Mg content of silicates and high Cr in spinel. Forsterite components of Ol mostly range from 90–92, with the high values up to 94.3. However, the observed variation in Mg contents in a single sample is not common in mantle residues; also, other lines of evidence do not support a residue origin of dunite. First, Ol commonly contains chromite inclusions (Figures 2D and 2E), which is not common in residual mantle peridotites. Second, our dunite contains low IPGE (<4.8 ppb) and low weight ratios of IPGE/PPGE (as low as 0.05) (Table 2), and the PGE contents and their normalized patterns are distinctly different from those of residual mantle peridotites (Figures 3A and 4). Rather, the PGE abundances and patterns are similar to cumulates (Figures 3B–3D and 4). Third, dunite xenoliths show young or even negative Re-depletion model ages (Xu *et al.* 2008), suggesting that the origin of the dunite is different from harzburgite, which has an Archaean model age. Considering these lines of evidence, we reject the possibility of residual mantle origin of dunite.

Dunite may form as a reaction product of peridotites with hydrous mafic melt. For example, it has been proposed that dunite in the mantle portions of many ophiolites was formed by interaction between infiltrating basaltic melt and peridotites, where pyroxene is replaced by Ol (Arai 1997; Morgan and Liang 2003). However, this possibility is not supported by the high Mg contents in Ol in our dunite; olivine produced from pyroxene during reaction with a primitive melt commonly shows variable and low Mg contents (e.g. Morgan and Liang 2003; Wang *et al.* 2008b). Furthermore, dunite formed through such reaction should retain the IPGE contents of their precursors because PGEs are essentially immobile, even during extensive metasomatism (Wang *et al.* 2008b). The contents of PGE and primitive mantle-normalized patterns for dunite xenoliths are significantly different from those of harzburgite. Therefore, we discount this possibility.

Finally, we suggest that the Laiwu dunite is a cumulate of a mafic melt. This is supported by the fine-grained textures and inclusions of chromite in Ol. The low concentrations of IPGE in Laiwu dunite provide strong evidence supporting its cumulate origin because these elements are retained in the residual mantle during partial melting (e.g. Righter *et al.* 2004; Brenan *et al.* 2005). The low concentrations of PGE in our dunite are not related to sulphide formation since there is no evidence indicating earlier formed sulphide minerals. Ol contains overall high contents of Ni, which shows a positive correlation with Mg, which suggests that S was insignificant during dunite formation

because sulphide would have incorporated Ni. It is unlikely that the dunite lost its PGE during late metasomatism since PGE, especially IPGE, are known to be immobile during high-temperature alteration and metasomatism. For example, highly metasomatized rocks, such as orthopyroxenite formed from harzburgite, retain their original PGE contents (e.g. Wang *et al.* 2008b). In addition, crustal rocks contain low concentrations of IPGE (e.g. Righter *et al.* 2004). Therefore, consistently low concentrations of IPGE in our samples and their PGE patterns, similar to Ural-Alaskan type dunite and pyroxenite (Figure 3), suggest that our dunite is a cumulate of mafic melt. This is further supported by similar PGE patterns between dunite and Ol-pyroxenite (Figure 3), because pyroxenite is clearly a cumulate. Xu *et al.* (2008) reported young or even negative Re-depletion model ages for dunite xenoliths, consistent with a cumulate origin of dunite from a mafic melt.

Nature of the parental magma for dunite

The contents of Al₂O₃ and TiO₂ in spinel are commonly used to estimate the composition of a melt since they are not affected by subsolidus re-equilibration with other minerals in ultramafic rocks (e.g. Kamenetsky *et al.* 2001). Chromites in the Laiwu dunite contain low TiO₂ and plot in the subduction-related magma field of Kamenetzky *et al.* (2001), similar to boninitic spinel (Dare *et al.* 2009) (Figure 7). Boninites commonly form in forearcs during the early stages of subduction, and almost always contain spinel with high Cr# (e.g. Crawford *et al.* 1989; Stern and Bloomer 1992), indicating that cumulates do not necessarily have low Cr# in spinel. In addition, Pagé and Barnes (2009) showed that cumulates commonly contain high Mg in Ol, high Cr# and low Ti in spinel in ophiolites compared to residual mantle harzburgites. Considering the tectonic history of the area, the parental melt for the dunite most likely formed during subduction of the Tethyan oceanic plate, probably in the early stage of its subduction.

The high Fo of Ol (up to 94.3) in the Laiwu dunite is explained by the reaction of Ol with earlier formed chromite in the cumulate, as spinel preferentially incorporates Fe (Bédard and Hébert 1998). Ol associated with chromitites commonly contains high Mg, up to Fo = 97 (e.g. Mussallam *et al.* 1981; Augé 1987). Earlier chromite formation is evident from abundant chromite inclusions in Ol grains in the dunite samples (Figure 2D and Figure 2E).

The proposed interpretation, dunite formed from subduction-related melt, suggests that it was generated earlier than the host Mg diorite because the latter formed after the collision of the Yangtze Craton and NCC (Gao *et al.* 2004, 2008; Xu *et al.* 2006, 2008). Our proposed interpretation is further supported by the occurrence of veinlets of orthopyroxenite in the dunite. The evidence suggests that the dunite formed earlier than the infiltration of Si-rich melt. The parental melt for the diorite was adakitic Si melt.

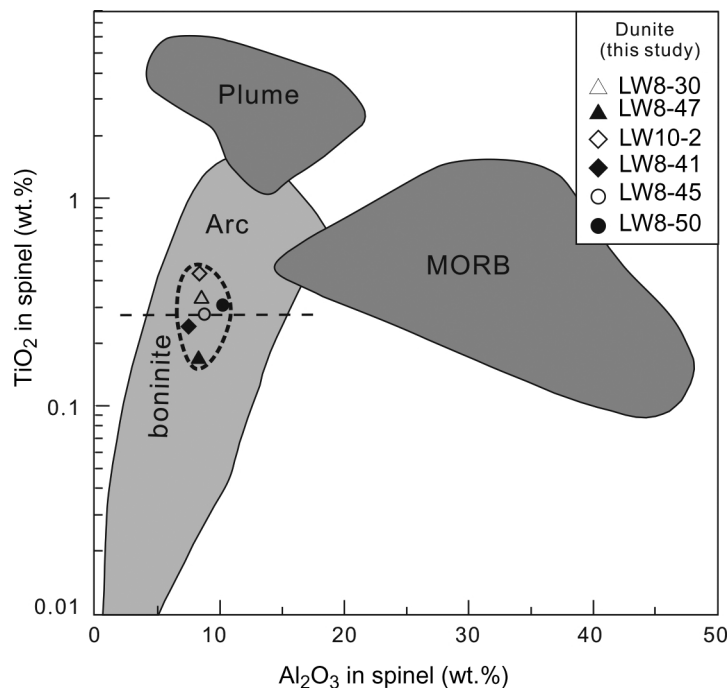


Figure 7. TiO_2 versus Al_2O_3 of spinel in volcanic rocks of Kamenetsky *et al.* (2001). The fields for large igneous provinces and oceanic island basalts form a 'plume' field. MORB, mid-ocean ridge basalt; Arc, subduction-related volcanic rocks. Spinel in boninites and boninitic rocks contain low TiO_2 (<0.35 wt.%) within the field of subduction-related rocks (e.g. Dare *et al.* 2009). The maximum TiO_2 is shown with a dashed line. Note that the chromite from Laiwu dunite plots in the boninite field. Symbols are the same as in Figure 4.

Conclusions

Ultramafic xenoliths in high-Mg diorites at Laiwu are mainly dunite (>80 vol.%) with minor harzburgite (<10 vol.%) and Ol-pyroxenite (<10 vol.%). Bulk rock compositions and mineral chemistry suggest that harzburgite is a residual peridotite after partial melting, whereas the low concentrations of IPGE suggest that the dunite is the cumulate of a mafic melt. High Cr in spinel further suggests that dunite formed as a cumulate of a boninitic melt, probably during the early stage of subduction of the Tethyan oceanic plate. High-Mg Ol grains (up to Fo 94.3) occur in the dunite, formed by interaction with chromite in the cumulate at depth.

Portions of the harzburgite and dunite were metasomatized by the infiltration of a Si-rich melt to produce secondary orthopyroxene after Ol, and variably low-Mg Ol. The metasomatism, in turn, likely resulted in Mg enrichment in the melt.

Ultramafic xenoliths have evidence of high $f\text{O}_2$, suggesting that the SCLM below the eastern margin of the NCC was oxidized; this oxidation probably occurred during the Mesozoic as a result of subduction of the Tethyan oceanic plate or marginal sediments on the Yangtze Craton during the collision of the Yangtze Craton and NCC.

Acknowledgements

We thank Smita Mohanty and Nimal DeSilva for the chemical analysis of samples at the University of Ottawa, and S. Zheng at

China University of Geosciences, Wuhan, for technical support during electron microprobe analysis. We also thank S. Arai for reading an earlier draft of the manuscript and constructive suggestions. We are grateful to Jeffrey Hedenquist for his helpful comments, which improved the clarity of this manuscript. Constructive comments by Gary Ernst and review by Guochun Zhao greatly improved the manuscript. This research was financially supported by a grant from the Natural Science and Engineering Research Council of Canada to KH and grants from the National Natural Science Foundation of China (numbers 90814003, 40873016, 41173034, 40573047). This research was also supported by a grant from China Geological Survey (number 1212011121088).

References

- Arai, S., 1997, Origin of podiform chromitites: *Journal of Asian Earth Sciences*, v. 15, p. 303–310.
- Augé, T., 1987, Chromite deposits in the northern Oman ophiolite: Mineralogical constraints: *Mineralium Deposita*, v. 22, p. 1–10.
- Ballhaus, C., 1993, Redox states of lithospheric and asthenospheric upper mantle: *Contributions to Mineralogy and Petrology*, v. 114, p. 331–348.
- Ballhaus, C., Berry, R.F., and Green, D.H., 1991, High pressure experiment calibration of the olivine-orthopyroxene-spinel oxygen barometer: Implications for the oxidation state of the mantle: *Contributions to Mineralogy and Petrology*, v. 107, p. 27–40.
- Barnes, S.J., and Roeder, P.L., 2001, The range of spinel compositions in terrestrial mafic and ultramafic rocks: *Journal of Petrology*, v. 42, p. 2279–2302.

- Bédard, J.H., and Hébert, R., 1998, Formation of chromitites by assimilation of crustal pyroxenites and gabbros into peridotitic intrusions: North Arm Mountain massif, bay of islands ophiolite, Newfoundland, Canada: *Journal of Geophysical Research*, v. 103, p. 5165–5184.
- Bell, D.R., Gregoire, M., Grove, T.L., Chatterjee, N., Carlson, R.W., and Buseck, P.R., 2005, Silica and volatile-element metasomatism of Archean mantle: A xenolith-scale example from the Kaapvaal Craton: *Contributions to Mineralogy and Petrology*, v. 150, p. 251–267.
- Brandon, A.D., and Draper, D.S., 1996, Constraints on the origin of the oxidation state of mantle overlying subduction zones: An example from Simcoe, Washington, USA: *Geochim et Cosmochim Acta*, v. 60, p. 1739–1749.
- Brenan, J.M., McDonough, W.F., and Ash, R., 2005, An experimental study of the solubility and partitioning of iridium, osmium and gold between olivine and silicate melt: *Earth and Planetary Science Letters*, v. 237, p. 855–872.
- Brey, G.P., and Köhler, T., 1990, Geothermobarometry in four-phase lherzolites: II. New thermobarometers and practical assessment of existing thermobarometers: *Journal of Petrology*, v. 31, p. 1353–1378.
- Bryndzia, L.T., and Wood, B.J., 1990, Oxygen thermobarometry of abyssal spinel peridotites: The redox state and C-H-O volatile composition of the Earth's sub-oceanic upper mantle: *The American Journal of Science*, v. 290, p. 1093–1116.
- Chen, L.H., and Zhou, X.H., 2005, Subduction-related metasomatism in the thinning lithosphere: Evidence from a composite dunite–orthopyroxenite xenolith entrained in Mesozoic Laiwu high-Mg diorite, North China Craton: *Geochem Geophys Geosyst*, v. 6, Q06008. doi: 10.1029/2005GC000938.
- Crawford, A.J., Falloon, T.J., and Green, D.H., 1989, Classification, petrogenesis and tectonic setting of boninites, in Crawford, A.J., ed., *Boninites and related rocks*: London, Unwin Hyman, p. 1–49.
- Dare, S.A.S., Pearce, J.A., McDonald, I., and Styles, M.T., 2009, Tectonic discrimination of peridotites using fO_2 -Cr# and Ga-Ti-Fe^{III} systematic in chrome-spinel: *Chemical Geology*, v. 261, p. 199–216.
- Dick, H.J.B., and Bullen, T., 1984, Chromian spinel as a petrogenetic indicator in abyssal and alpine-type peridotites and spatially associated lavas: *Contributions to Mineralogy and Petrology*, v. 86, p. 54–76.
- Eggins, S.M., Rudnick, R.L., and McDonough, W.F., 1998, The composition of peridotites and their minerals: A laser-ablation ICP-MS study: *Earth and Planetary Science Letters*, v. 154, p. 53–71.
- Engelbreton, D.C., Cox, A., and Gordon, R.G., 1985, Relative motions between oceanic and continental plates in the Pacific basins: *Geological Society, America, Special Papers*, v. 206, p. 1–59.
- Fan, W.M., Zhang, H.F., Baker, J., Jarvis, K.E., Mason, P.R.D., and Menzies, M.A., 2000, On and off the North China Craton: Where is the Archaean keel?: *Journal of Petrology*, v. 41, p. 933–950.
- Gao, S., Rudnick, R.L., Xu, W.L., Yuan, H.L., Liu, Y.S., Puchtel, I., Liu, X., Huang, H., and Wang, X.R., 2008, Recycling deep cratonic lithosphere and generation of intraplate magmatism: *Earth and Planetary Science Letters*, v. 270, p. 41–53.
- Gao, S., Rudnick, R.L., Yuan, H.L., Liu, X.M., Liu, Y.S., Xu, W.L., Ling, W.L., Ayers, J., Wang, X.C., and Wang, Q.H., 2004, Recycling lower continental crust in the North China Craton: *Nature*, v. 432, p. 892–897.
- Garuti, G., Fershtater, G., Bea, F., Montero, P., Pushkarev, E.V., and Zaccarini, F., 1997, Platinum-group elements as petrological indicators in mafic-ultramafic complexes of the central and southern Urals: Preliminary results: *Tectonophysics*, v. 76, p. 181–194.
- Griffin, W.L., Zhang, A.D., O'Reilly, S.Y., and Ryan, C.G., 1998, Phanerozoic evolution of the lithosphere beneath the Sino-Korean Craton, in Flower, M.J.F., et al., eds., *Mantle dynamics and plate interactions in East Asia*, *Geodynamic Series*, v. 27: Washington, DC, AGU, p. 107–126.
- Hattori, K.H., and Guillot, S., 2007, Geochemical character of serpentinites associated with high- to ultrahigh-pressure metamorphic rocks in the Alps, Cuba, and the Himalayas: Recycling of elements in subduction zones: *Geochemistry Geophysics and Geosystems*, v. 8, Q09010. doi: 10.1029/2007GC001549.
- Hattori, K.H., Wallis, S., Enami, T., and Mizukami, T., 2010, Subduction of mantle wedge peridotites: Evidence from the Higashi-akaishi ultramafic body in the Sanbagawa metamorphic belt: *Island Arc*, v. 19, p. 192–207.
- Ishii, T., Robinson, P.T., Maekawa, H., and Fiske, R., 1992, Petrological studies of peridotites from diapiric serpentinites seamounts in the Izu-Ogasawara-Mariana forearc, Leg 125, in Fryer, P., Pearce, J.A., Stokking, L.B., et al., eds., *Proceedings of Ocean Drilling Program Scientific Results: College Station, TX, Ocean Drilling Program*, v. 125, p. 445–485. doi:10.2973/odp.proc.sr.125.129.1992.
- Kamenetsky, V.S., Crawford, A.J., and Meffre, S., 2001, Factors controlling chemistry of magmatic spinel: An empirical study of associated olivine, Cr spinel and melt inclusions from primitive rocks: *Journal of Petrology*, v. 42, p. 655–671.
- Kelemen, P.B., Joyce, D.B., Webster, J.D., and Holloway, J.R., 1990, Reaction between ultramafic rock and fractionating basaltic magma II. Experimental investigation of reaction between olivine tholeiite and harzburgite at 1150°–1050°C and 5 Kb: *Journal of Petrology*, v. 31, p. 99–134.
- Kubo, K., 2002, Dunite formation processes in highly depleted peridotites: Case study of the Iwanaidake peridotite, Hokkaido, Japan: *Journal of Petrology*, v. 43, p. 423–448.
- Kusky, T.M., Windley, B.F., and Zhai, M.G., 2007, Lithospheric thinning in eastern Asia: Constraints, evolution, and tests of models: *Geological Society, London, Special Publications*, v. 280, p. 331–343.
- Leblanc, M., and Ceuleneer, G., 1992, Chromite crystallization in a multi-cellular magma flow: Evidence from a chromitite dike in the Oman ophiolite: *Lithos*, v. 27, p. 231–257.
- Li, S.Z., Kusky, T.M., Zhao, G.C., Wu, F.Y., Liu, J.Z., Sun, M., and Wang, L., 2007, Mesozoic tectonics in the Eastern block of the North China Craton: Implications for subduction of the Pacific plate beneath the Eurasian plate: *Geological Society, London, Special Publications*, v. 280, p. 171–188.
- Liu, X.W., Jin, Z.M., and Green, H.W., 2007, Clinostatite exsolution in diopsidic augite of Dabieshan: Garnet peridotite from depth of 300 km: *The American Mineralogist*, v. 92, p. 546–552.
- McCammon, C., and Kopylova, M.G., 2004, A redox profile of the Slave mantle and oxygen fugacity control in the cratonic mantle: *Contributions to Mineralogy and Petrology*, v. 148, p. 55–68.
- McDonough, W.F., and Sun, S.S., 1995, The composition of the Earth: *Chemical Geology*, v. 120, p. 223–253.
- Meisel, T., and Moser, J., 2004, Reference materials for geochemical PGE analysis: New analytical data for Ru, Rh, Pd, Os, Ir, Pt and Re by isotope dilution ICP-MS in 11 geological reference materials: *Chemical Geology*, v. 208, p. 319–338.

- Morgan, Z., and Liang, Y., 2003, An experimental and numerical study of the kinetics of harzburgite reactive dissolution with applications to dunite dike formation: *Earth and Planetary Science Letters*, v. 214, p. 59–74.
- Mussallam, K., Jung, D., and Burgath, K., 1981, Textural features and chemical characteristics of chromites in ultramafic rocks, Chalkidiki complex (northeastern Greece): *Tschermaks Mineralogische und Petrographische Mitteilungen*, v. 29, p. 75–101.
- Pagé, P., and Barnes, S.-J., 2009, Using trace elements in chromites to constrain the origin of podiform chromitites in the Thetford Mines ophiolite, Québec, Canada: *Economic Geology*, v. 104, p. 997–1018.
- Parkinson, I.J., and Arculus, R.J., 1999, The redox state of subduction zones: Insights from arc-peridotites: *Chemical Geology*, v. 160, p. 409–423.
- Parkinson, I.J., Arculus, R.J., and Eggins, S.M., 2003, Peridotite xenoliths from Grenada, lesser Antilles Island arc: *Contributions to Mineralogy and Petrology*, v. 146, p. 241–262.
- Rehkämper, M., Halliday, A.N., and Alt, J., 1999, Non-chondritic platinum-group elements ratios in oceanic mantle lithosphere: Petrogenetic signature of melt percolation?: *Earth and Planetary Science Letters*, v. 127, p. 65–81.
- Righter, K., Campbell, A.J., Humayun, M., and Hervig, R.L., 2004, Partitioning of Ru, Rh, Pd, Re, Ir and Au between Cr-bearing spinel, olivine, pyroxene and silicate melts: *Geochimica et Cosmochimica Acta*, v. 68, p. 867–880.
- Saumur, B.-J., Hattori, K.H., and Guillot, S., 2011, Contrasting origins of serpentinites in a subduction complex, northern Dominican Republic: *Geological Society of America Bulletin*, v. 122, p. 292–304.
- Shellnutt, J.G., and Zellmer, G.F., 2010, High-Mg andesite genesis by upper crustal differentiation: *Journal of the Geological Society*, v. 167, p. 1081–1088.
- Shirai, N., Nishino, T., Li, X., Amakawa, H., and Ebihara, M., 2003, Precise determination of PGE in a GSJ reference sample JP-1 by ID-ICPMS after nickel sulfide fire assay preconcentration: *Geochemical Journal*, v. 37, p. 531–536.
- Stern, R.J., and Bloomer, S.H., 1992, Subduction zone infancy: Examples from the Eocene Izu-Bonin-Mariana and Jurassic California arcs: *Geological Society of America Bulletin*, v. 104, p. 1621–1636.
- Wang, J., Hattori, K.H., Li, J.P., and Stern, C., 2008a, Oxidation state of paleozoic subcontinental lithospheric mantle below the Pali Aike volcanic field in southernmost Patagonia: *Lithos*, v. 105, p. 98–110.
- Wang, J., Hattori, K.H., and Stern, C., 2008b, Metasomatic origin of garnet orthopyroxenites in the subcontinental lithospheric mantle underlying Pali Aike volcanic field, southern South America: *Mineralogy and Petrology*, v. 94, p. 243–258.
- Wells, P.R.A., 1977, Pyroxene thermometry in simple and complex systems: *Contributions to Mineralogy and Petrology*, v. 62, p. 119–139.
- Wood, B.J., and Virgo, D., 1989, Upper mantle oxidation state: Ferric iron contents of Iherzolite spinels by ^{57}Fe Mössbauer spectroscopy and resultant oxygen fugacities: *Geochim et Cosmochim Acta*, v. 53, p. 1277–1291.
- Woodland, A.B., and Koch, M., 2003, Variation in oxygen fugacity with depth in the upper mantle beneath Kaapvaal craton, South Africa: *Earth and Planetary Science Letters*, v. 214, p. 295–310.
- Wu, F.Y., Lin, J.Q., Wilde, S.A., Zhang, X.O., and Yang, J.H., 2005, Nature and significance of the Early Cretaceous giant igneous event in eastern China: *Earth and Planetary Science Letters*, v. 233, p. 103–119.
- Wu, F.Y., Sun, D.Y., Ge, W.C., Zhang, Y.B., Grant, M.L., Wilde, S.A., and Jahn, B.M., 2011, Geochronology of the Phanerozoic granitoids in northeastern China: *Journal of Asian Earth Sciences*, v. 41, p. 1–30.
- Xiao, W.J., Windley, B.F., Hao, J., and Zhai, M.G., 2003, Accretion leading to collision and the Permian Solonker suture, Inner Mongolia, China: Termination of the Central Asian orogenic belt: *Tectonics*, v. 22, p. 1069. doi: 10.1029/2002.TC001484.
- Xu, W.L., Gao, S., Wang, Q.H., Wang, D.Y., and Liu, Y.S., 2006, Mesozoic crustal thickening of the eastern North China Craton: Evidence from eclogite xenoliths and petrologic implications: *Geology*, v. 34, p. 721–724.
- Xu, W.L., Hergt, J.M., Gao, S., Pei, F., Wang, W., and Yang, D., 2008, Interaction of adakitic melt-peridotite: Implications for the high-Mg# signature of Mesozoic adakitic rocks in the eastern North China craton: *Earth and Planetary Science Letters*, v. 265, p. 123–137.
- Xu, W.L., Wang, D.Y., Gao, S., and Lin, J.Q., 2003, Discovery of dunite and pyroxenite xenoliths in Mesozoic diorite at Jinling, western Shandong and its significance: *Chinese Science Bulletin*, v. 48, p. 1599–1604.
- Xu, W.L., Wang, D.Y., Wang, Q.H., Gao, S., and Lin, J.Q., 2004a, Metasomatism of silica-rich melts (liquids) in dunite xenoliths from western Shandong, China: Implication for Mesozoic lithospheric mantle thinning: *Acta Geologica Sinica*, v. 78, p. 72–80 (in Chinese with English abstract).
- Xu, Y.G., Huang, X.L., and Ma, J.L., 2004b, Crust-mantle interaction during the tectono-thermal reactivation of the North China Craton: Constraints from SHRIMP zircon U-Pb chronology and geochemistry of Mesozoic plutons from western Shandong: *Contributions to Mineralogy and Petrology*, v. 147, p. 750–767.
- Yang, C.H., 2008, Chronology and geochemistry of Mesozoic high-Mg diorites in western Shandong: Constraints on lithospheric evolution of the North China Craton [Ph.D. thesis]: Changchun, Jilin University, China, p.41–100.
- Yang, E.X., Wang, S.J., Zhang, C.C., and Ren, T.L., 2004, Discovery and significance of Neogene period Shanwang Formation in Laiwu basin, Shandong Province: *Geological Survey and Research*, v. 27, no.1, p. 48–51 (in Chinese with English abstract).
- Ye, K., Cong, B.L., and Ye, D.N., 2000, The possible subduction of continental material to depths greater than 200 km: *Nature*, v. 407, p. 734–736.
- Zhai, M.G., 2004, Precambrian tectonic evolution of the North China Craton, in Malpas J., Fletcher C.J.N., Ali J.R., and Aitchison J.C., eds., *Aspects of the tectonic evolution of China*, v. 226: London, Geological Society Special Publications, p. 57–72.
- Zhang, H.F., Goldstein, S.L., Zhou, X.H., Sun, M., Zheng, J.P., and Cai, Y., 2008, Evolution of subcontinental lithospheric mantle beneath eastern China: Re-Os isotopic evidence from mantle xenoliths in Paleozoic kimberlites and Mesozoic basalts: *Contributions to Mineralogy and Petrology*, v. 155, p. 271–293.
- Zhang, H.F., and Sun, M., 2002, Geochemistry of Mesozoic basalts and mafic dikes, southeastern North China Craton, and tectonic implications: *International Geology Review*, v. 44, p. 370–382.
- Zhang, H.F., Sun, M., Zhou, X.H., Fan, W.M., Zhai, M.G., and Yin, J.F., 2002, Mesozoic lithosphere destruction beneath the North China Craton: Evidence from major, trace element, and Sr-Nd-Pb isotope studies of Fangcheng basalts: *Contributions to Mineralogy and Petrology*, v. 144, p. 241–253.

- Zhang, R.Y., and Liou, J.G., 2003, Clinopyroxene from the Sulu garnet clinopyroxenite, China: Origin and evolution of garnet exsolution in clinopyroxene: *The American Mineralogist*, v. 88, p. 1591–1619.
- Zhao, G.C., Sun, M., Wilde, S.A., and Li, S.Z., 2005, Late Archean to Paleoproterozoic evolution of the North China Craton: Key issues revisited: *Precambrian Research*, v. 136, p. 177–202.
- Zhao, G.C., Wilde, S.A., Cawood, P.A., and Sun, M., 2001, Archean blocks and their boundaries in the North China Craton: Lithological, geochemical, structural and P–T path constraints and tectonic evolution: *Precambrian Research*, v. 107, p. 45–73.
- Zheng, J.P., Griffin, W.L., O'Reilly, S.Y., Yu, C.M., Zhang, H.F., Pearson, N., and Zhang, M., 2007, Mechanism and timing of lithospheric modification and replacement beneath the eastern North China Craton: Peridotitic xenoliths from the 100 Ma Fuxin basalts and a regional synthesis: *Geochimica et Cosmochimica Acta*, v. 71, p. 5203–5225.
- Zhou, M.F., Robinson, P.T., Malpas, J., and Li, Z., 1996, Podiform chromitites in the Luobusa ophiolite (Southern Tibet): Implications for melt-rock interaction and chromite segregation in the upper mantle: *Journal of Petrology*, v. 37, p. 3–21.
- Zhou, M.F., Sun, M., Keays, R.R., and Kerrich, R.W., 1998, Controls on platinum-group elemental distributions of podiform chromitites: A case study of high-Cr and high-Al chromitites from Chinese orogenic belts: *Geochimica et Cosmochimica Acta*, v. 62, p. 677–688.